RSC Advances

PAPER

View Article Online
View Journal | View Issue

Cite this: *RSC Adv.*, 2017, **7**, 32721

Synthesizing nonstoichiometric $Li_{3-3x}V_{2+x}(PO_4)_3$/C as cathode materials for high-performance lithium-ion batteries by solid state reaction†

Pingping Sun,[a] Ningang Su,[a] Yuanting Wang,[a] Qingyu Xu,*[ab] Qi Fan*[c] and Yueming Sun[c]

Received 30th April 2017
Accepted 23rd June 2017

DOI: 10.1039/c7ra04842d

rsc.li/rsc-advances

A simple solid state reaction method has been developed to synthesize nonstoichiometric $Li_{3-3x}V_{2+x}(PO_4)_3$/C (x = 0–0.15) nanocomposites. Among them, $Li_{3-3x}V_{2+x}(PO_4)_3$/C nanocomposites with x = 0.10 exhibit the best performance, especially notable for its high-rate performance. The discharge capacity of 124.3 mA h g^{-1} is delivered at 20C, almost 1.5 times that of stoichiometric $Li_3V_2(PO_4)_3$/C nanocomposites cathode (85 mA h g^{-1}). Long-life cycling performance at a high rate of 20C is also exhibited, retaining 98.3% of its original discharge capacity (124.3 mA h g^{-1}) after 1000 cycles. The cyclic voltammetry and AC impedance analysis indicate that the $Li_{3-3x}V_{2+x}(PO_4)_3$/C (x = 0.10) composites show the best ionic diffusivity and lowest resistance.

1. Introduction

Rechargeable lithium-ion batteries (LIBs) have been rapidly developed for applications in electric vehicles, hybrid electric vehicles, and large-scale energy storage because of their high energy density and durable cycle life.[1–3] But developing an electric battery with low cost, fast charge/discharge rate, high capacity/power and long lifespan is still a significant challenge.[4,5] Monoclinic $Li_3V_2(PO_4)_3$ has been proposed as next-generation cathode material for lithium ion batteries due to its excellent thermal stability, large reversible capacity, high operating potential, and relatively rapid ionic mobilities.[6–8] However, $Li_3V_2(PO_4)_3$ suffers a poor electronic conductivity (2.4×10^{-7} S cm^{-1} at room temperature) due to the nature of its separated VO_6 octahedral arrangement, which significantly limits its rate performance and the further commercialization.[9–11] Carbon coating and doping have been proved to be efficient in boosting the rate and cycle performance of $Li_3V_2(PO_4)_3$.[12–16] Current strategies used for the preparation of high performance $Li_3V_2(PO_4)_3$ include electrospin,[8] hydrothermal self-assembly,[9] freeze-drying method,[13] and ionic-liquid assisted synthesis.[10] Although these methods have their own advantages, they are much limited by high cost and complicated procedures and not suitable for large-scale production. High energy ball milling (HEBM) emerged as an efficient technique to produce nanomaterials has been widely used in the preparation of phosphates.[17–23] In our previous work, we synthesized nonstoichiometric $Li_{2.7}V_{2.1}(PO_4)_3$ by tuning the Li deficiency and V excess through a sol–gel procedure followed by HEBM.[24] The electrochemical performance is significantly improved and the rate performance enhancement has been ascribed to the shell of active layer $LiVOPO_4$ (denoted as LVOP). However, the procedure of mixed solution of all the sources will inevitably produce much waste water, leading to the potential environment pollution. Solid state reaction by mixing the reaction sources directly is a more convenient industrial technique. Based on the above high rate performance of nonstoichiometric $Li_{3-3x}V_{2+x}(PO_4)_3$ samples (LVP-x), we further prepared the samples with various V concentrations by solid state reaction. Consistent with previous results, LVP-x nanocomposite with x = 0.10 exhibits the most excellent performance.[24,25] It presents high rate performance of 124.3 mA h g^{-1} even at 20C, almost 1.5 times of that of the LVP-0 cathode (85 mA h g^{-1}). Long-life cycling performance at high rate of 20C is also exhibited, retaining 98.3% of its original discharge capacity after 1000 cycles. By using this solid state reaction method, the cell performance is significantly improved, compared with that prepared by the sol–gel method.[24]

2. Experimental section

2.1. Synthesis of LVP-x (x = 0–0.15) nanocomposites

LVP-x (x = 0–0.15) nanocomposites were prepared by solid state reaction. In a typical process, appropriate amount of NH_4VO_3 (AR, ≥99.0%), $LiOH \cdot H_2O$ (AR, ≥99.0%), $NH_4H_2PO_4$ (AR, ≥99.0%) and citric acid (AR, ≥99.5%) were mixed and high-energy ball milled for 0.5 hours. The mixture was transferred

[a]Department of Physics, Southeast University, Nanjing 211189, China. E-mail: xuqingyu@seu.edu.cn
[b]National Laboratory of Solid State Microstructures, Nanjing University, Nanjing 210093, China
[c]College of Chemistry and Chemical Engineering, Southeast University, Nanjing 211189, China. E-mail: fanqi1984@126.com

† Electronic supplementary information (ESI) available. See DOI: 10.1039/c7ra04842d

to a quartz tubular furnace and heated at 350 °C for 6 hours in Ar flow. Then the precursors were high energy ball milled again, and finally sintered at 800 °C for 4 hours in Ar flow.

2.2. Structural characterizations

The structure of LVP-x was characterized by X-ray diffraction (XRD, Rigaku Smartlab 3) and transmission electron microscope (TEM, FEI Tecnai F20). Morphologies were studied by a scanning electron microscope (SEM, FEI Inspect F50). X-ray photoelectron spectroscopy (XPS) was carried out using an X-ray photoelectron spectrometer (ThermoFisher SCIENTIFIC) with Al Kα X-ray source ($h\nu$ = 1486.6 eV). The samples for XPS measurements were kept in the high-vacuum chamber overnight to remove the absorbed air.

2.3. Electrochemical characterizations

Electrochemical measurements were performed using CR2025 coin cells. The electrodes were prepared by blending the LVP-x with acetylene black, carbon nanotube (CNT) and polyvinylidene fluoride (PVDF) binder with weight ratio of 80 : 10 : 5 : 5 in N-methylpyrrolidone (NMP). The slurry of mixture was coated onto an aluminum foil using a manually adjustable film-coating equipment and dried in a vacuum oven at 120 °C for 12 hours. The dried positive electrode sheet was cut into discs with diameter of 12 mm, and then pressed under a fixed pressure. The coin cells were assembled in an argon-filled glove box. Pure lithium foil was used as the counter and reference electrode, a polypropylene separator (Celgard 2400) was used to separate the cathode and anode with 1 mol L^{-1} $LiPF_6$ in ethylene carbonate (EC) : dimethyl carbonate (DMC) (1 : 1 v/v ratio) as the electrolyte. Galvanostatic charging/discharging tests were taken in a voltage cut-off of 3.0 to 4.3 V (*vs.* Li/Li^+) at various C-rates on a NEWARE battery testing system at room temperature. Cyclic voltammetry (CV) and Electrochemical impedance spectroscopy (EIS) measurements were performed on CHI 660A electrochemical analyzer workstation (Chenhua, Shanghai, China). For the EIS measurements, the amplitude of AC voltage on cells was 5 mV and the frequency range was between 100 kHz and 10 MHz.

3. Results and discussion

Fig. 1 shows the XRD patterns of LVP-x (x = 0–0.15) composites. The samples were identified to be the monoclinic LVP and orthorhombic LVOP, as our previous work reported that the composite is consisted of core LVP and shell LVOP.[24] The mass content of each phase in composites is obtained through Rietveld refinement (Table 1). With increasing the content of V, the mass of the shell LVOP increase at the same time. There are no diffraction peaks corresponding to carbon left in LVP-x, indicating the amorphous nature of residual carbon.

Fig. 2 shows the SEM images of the LVP-x samples. There is no significant size dependence on the nonstoichiometric concentration. From the pictures, we can see that the particle sizes for the LVP-x are almost the same as those of $x \leq 0.10$, but larger particle size can be observed with further increasing x up to 0.15. Furthermore, it can be seen that the particles of the

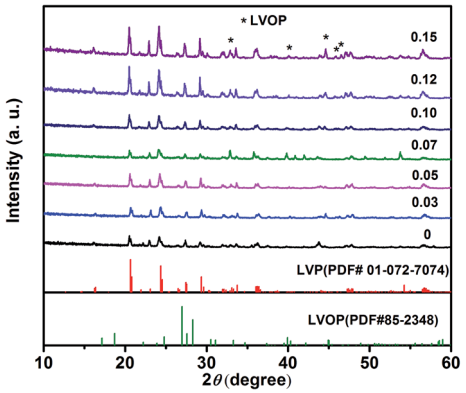

Fig. 1 XRD patterns of LVP-x (x = 0–0.15).

Table 1 Refined unit cell for LVP-x (x = 0–0.15) composites

	Mass content/%		
Samples	$Li_3V_2(PO_4)_3$	$LiVOPO_4$	R_p (%)
LVP-0	100	0	3.83
LVP-0.03	99.30	0.70%	13.13
LVP-0.05	98.43	1.57%	13.35
LVP-0.07	97.14	2.86%	14.96
LVP-0.10	96.41	3.59%	14.84
LVP-0.12	95.60	4.40%	11.03
LVP-0.15	94.85	5.15%	12.28

samples merge with each other and form a porous network. This geometry has several advantages such as good accommodation of volume changes without fracture during cycling, good electrical connection with the current collector and efficient for electron transportation. This microstructure is beneficial for the electrolyte to penetrate into the positive materials, which is promoted for good electronic contact among the composites particles.

A typical HRTEM image (Fig. S1†) is presented to investigate the structure of LVP-0.10. Two types of lattice fringes are found in the composites: the $Li_3V_2(PO_4)_3$ lattice fringe with an interplanar spacing of 0.3794 nm that corresponds to the (210) lattice planes; and the $LiVOPO_4$ lattice fringe with an interplanar spacing of 0.3858 nm that corresponds to the (111) lattice planes. Fast fourier transform (FFT) was performed in the selected crystal planes to confirm the different phases, as shown in inset. The FFT images of the selected regions show the diffraction peaks of $Li_3V_2(PO_4)_3$ and $LiVOPO_4$, respectively. Different diffraction patterns are obtained, indicating that two phases coexist in the samples. The HRTEM image confirms the $Li_3V_2(PO_4)_3$ core and $LiVOPO_4$ shell structure, similar to our previous results.[24]

XPS is provided to detect the surface phase of each particle. V2p peaks of LVP-0.10 (Fig. S2†) prepared by solid state reaction significantly shifts to higher binding energy, compared with that prepared by sol–gel method,[25] and are close to that made by sol–gel with ball mill method.[24] The binding energies are consistent with those of V^{4+} in $LiVOPO_4$.

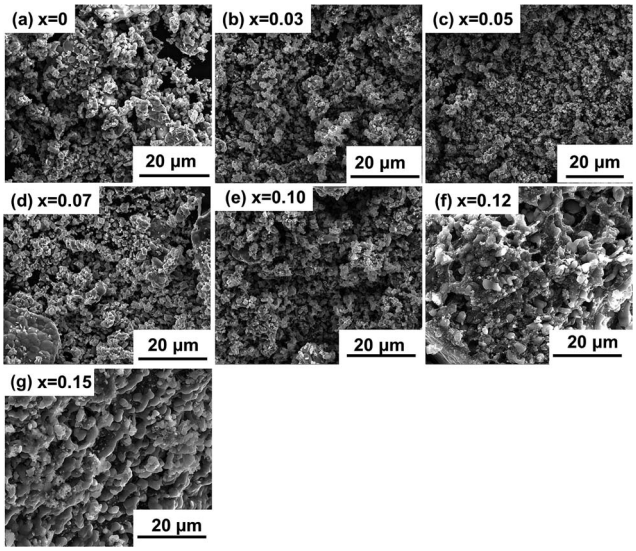

Fig. 2 SEM images of LVP-x (x = 0–0.15).

The Li storage performances were investigated by using coin-type cells. From Fig. 3a, LVP-0.10 exhibits three pairs of charge/discharge plateaus. The three charge plateaus located around 3.60 V, 3.68 V and 4.09 V can be identified as the extraction of Li ions from $Li_3V_2(PO_4)_3$ to $LiV_2(PO_4)_3$ and the corresponding phase transition processes during the electrochemical reactions. Meanwhile, during the discharge process, three plateaus located at around 4.04 V, 3.65 V and 3.57 V can be attributed to the insertion of the extracted Li ions, which is accompanied by the phase transition from $LiV_2(PO_4)_3$ to $Li_3V_2(PO_4)_3$.[10,11]

Rate performance of all samples was further studied. With increasing current rate, LVP-0.10 exhibits the smallest capacity decay among all the samples (Fig. 3b). When the rate is increased to 10C, a discharge capacity of 124.6 mA h g^{-1} (94% of the theoretical capacity) is still delivered, indicating an excellent high-rate capability. Even at 20C, a discharge capacity of 124.3 mA h g^{-1} is delivered, almost 1.5 times of that of LVP-0 cathode (85 mA h g^{-1}), indicating the excellent high-rate capability. After rapid changes of current rate, the LVP-0.10 cathode shows stable capacities at each step. When the rate is turned back to 0.5C, a discharge capacity of 129.8 mA h g^{-1} (LVP-0.10) is recovered, much higher than 95.3 mA h g^{-1} (LVP-0), indicating very good electrochemical reversibility. Long-life cycling performance of samples at high rate of 20C is subsequently shown in Fig. 3c. LVP-0.10 cathode exhibits an initial discharge capacity of 124.3 mA h g^{-1} (only 85 mA h g^{-1} for LVP-0), and delivers a remarkable capacity of 122.2 mA h g^{-1} after 1000 cycles (only 76.6 mA h g^{-1} for LVP-0), corresponding to capacity retention of 98.3%. The electrochemical performance of the sample we prepared is the best among all LVP composites (Tables S1 and S2†). The above electrochemical measurements indicate another important advantage of the nonstoichiometric strategy that the performance of LVP-x with broad x distribution from 0.03 to 0.15 has been improved compared with that of stoichiometric LVP. This definitely will benefit the large-scale industrial production which can tolerate larger composition variation in the final products.

To reveal the underlying mechanism of enhanced electrochemical performance for LVP-0.10, CV and EIS were measured. The peak current increases with increasing scanning rate, meanwhile the cathodic and anodic peaks shift to lower and higher potentials, respectively (Fig. 4a). Compared with the peak shift of LVP-0 cathode (Fig. 4b), LVP-0.10 cathode undergoes three complete phase transitions with higher current, indicating higher reversibility and faster kinetics during electrochemical reaction. The Li^+ ion diffusion coefficients were calculated, based on Randles–Sevcik equation (eqn (1)) for semi-infinite diffusion of Li^+ into LVP,[26]

$$I_p = 2.69 \times 10^5 n^{3/2} A C_0 D^{1/2} v^{1/2} \quad (1)$$

where I_p is the peak current, n the number of electrons transferred per molecule during the intercalation, A the surface area of active electrode, C_0 the concentration of Li^+ ions in the cathode, D the diffusion coefficient of Li^+ ions, and v the scanning rate. From the slope of fitting line collected from peak b (Fig. 4c), the diffusion coefficient D of LVP-0.10 is 1.84×10^{-9} cm^2 s^{-1}, much higher than that of LVP-0 (5.37×10^{-10} cm^2 s^{-1}). Li diffusivity can be dramatically enhanced when the material is

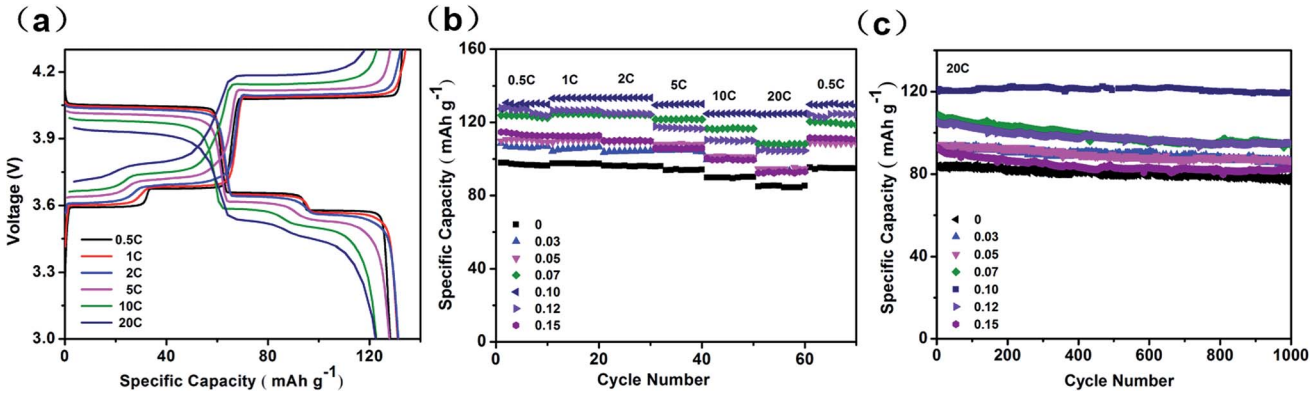

Fig. 3 (a) Charge–discharge profiles of LVP-0.10 at different current rates. (b) Rate performance of LVP-x (x = 0–0.15). (c) Life cycling performance of LVP-x (x = 0–0.15) at 20C.

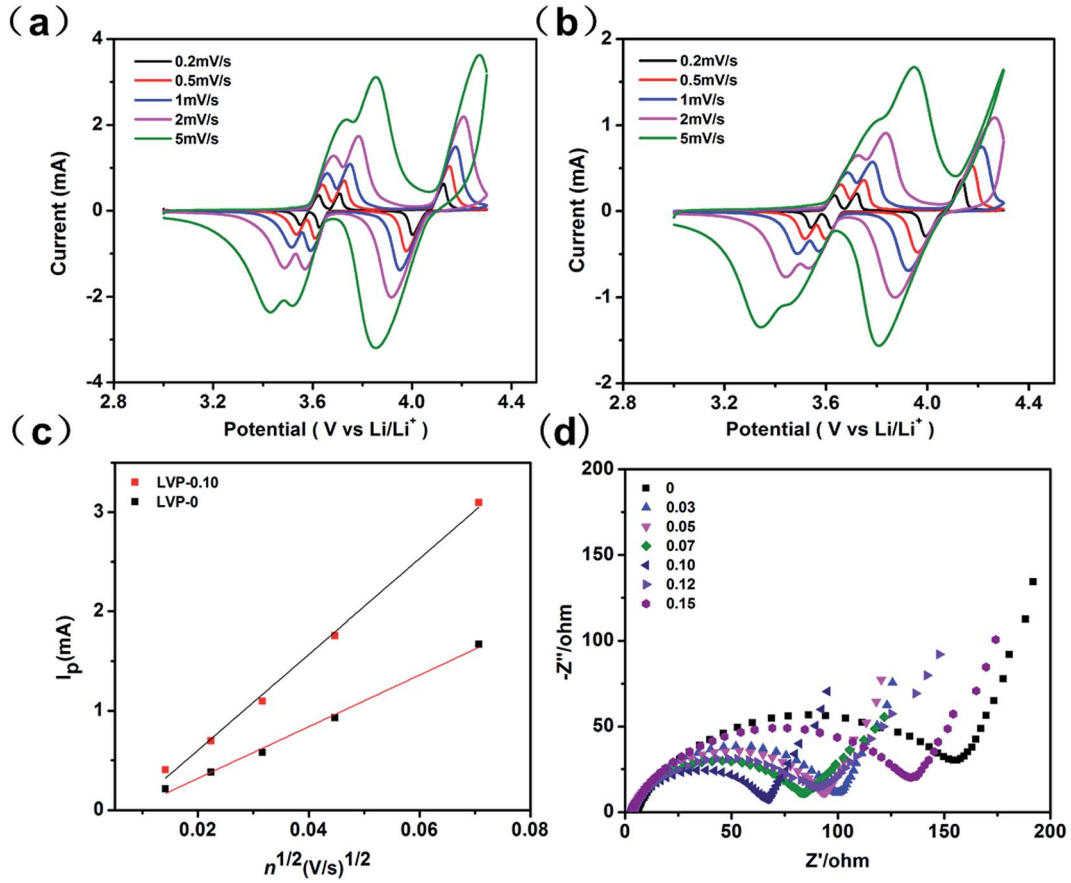

Fig. 4 CV of (a) LVP-0.10 and (b) LVP-0 at different scanning rates. (c) Linear fitting of I_p *vs.* $v^{1/2}$ curves for the peak b. (d) Nyquist plots of LVP-*x* (*x* = 0–0.15) before cycles.

mechanically treated in a high-energy ball mill.[27] For example, the diffusion coefficient D of the sample LVP-0.10 prepared by sol–gel method is 1.45×10^{-9} cm^2 s^{-1},[25] and 1.04×10^{-9} cm^2 s^{-1} for LVP-0.10 obtained by combining sol–gel and high energy ball milling method.[24] Although the grain size is not drastically reduced after a short milling time, mechanical treatment has a large effect on the transport parameters. M. Wilkening *et al.* proposed that a high defect concentration in the interior and/or on the surface of the grains is generated by HEBM, which seems to contribute also to the large increase of Li^+ ion conductivity.[27] The Nyquist plots (Fig. 4d) show the charge transfer resistance (R_{ct}) of LVP-*x* (*x* = 0–0.15). Among all the samples, LVP-0.10 shows the smallest charge transfer resistance (62.4 Ω), indicating LVP-0.10 provides highest efficient electron/ion transport than others. Even after 1000 cycles, the impedance variation of LVP-0.10 electrode demonstrates a depressed semicircle at high-to-medium frequencies and a sloped line at low frequencies, as shown in Fig. 5. The R_{ct} value decreased from 62.4 Ω to 29.2 Ω for LVP-0.10, and from 153.2 to 97.6 Ω for LVP-0, due to the decreased solid electrolyte interface (SEI) resistance,[28] demonstrating that the core–shell LVP-0.10 phase provides higher efficient electron/ion transport than that of LVP-0. and resulting in excellent electrochemical performance. On the basis of above results, the superior high-rate and ultra-long cycling performance of LVP-0.10 has been attributed to the improved electron/ion conductivity which greatly facilitates the ion diffusion kinetics and reduced R_{ct}.

Synthesis process plays a major role in improving the physicochemical properties of the electrode materials. Table S3† compares the electrochemical kinetic parameters among $Li_3V_2(PO_4)_3$ nanocomposites of previous and present work. The sample prepared by solid state method shows improved Li^+ and

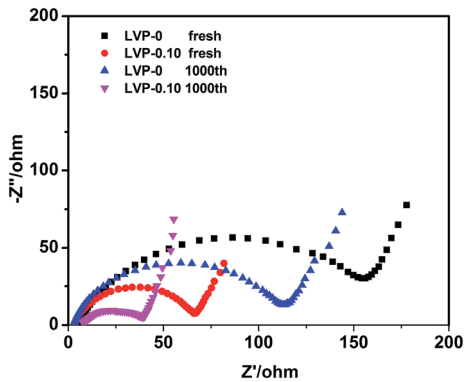

Fig. 5 Nyquist plots of the LVP-0 and LVP-0.10 fresh and after 1000 cycles.

electron conductivity, accounting for the excellent high rate and long cycle performance. In our previous work, we synthesized nonstoichiometry LVP-*x* by sol–gel method,[24,25] and obtained excellent electrochemical performance. The former method offers products with a homogeneous distribution of uniform, sub-micron size particles, whereas the latter usually lead to more inhomogeneous.[29] The inhomogeneity resulting in composition variation plays a similar role as nonstoichiometric modulation. This needs to be further verified by advanced structural characterization. Also, high defect concentration in the interior and/or on the surface of the grains is generated by HEBM, which seems to contribute also to the large increase of Li conductivity.[27,30] A LVP-core and LVOP shell structure has been formed by HEBM treatment on nonstoichiometric LVP, and the higher capacity of LVOP shell improves the high-rate performance.[24] LVP-0.10 shows the best electrochemical performance among all the samples, while further increase *x* the electrochemical performance decreases. This indicates that it has an optimized thickness for LVOP shell on the surface of LVP particles. Because too thick shell may hinder the Li^+/e^- transport in the charge/discharge process caused by the poor electronic conductivity of LVOP. On the other hand, the results obtained from solid state reaction is consistent with that from sol–gel method, that LVP-0.10 shows the best electrochemical performance among all the samples, demonstrating it is an efficient strategy to enhance the electrochemical performance of LVP by nonstoichiometric modulation.

4. Conclusion

In summary, we have developed a cost-efficient strategy of nonstoichiometry to synthesize high-rate and ultralong-life performance cathode of LVP-*x* by solid state reaction method. This approach is convenient and cost-saving since it is a one-step technique by *in situ* carbonization along with the crystallization of LVP without using any hard templates and surfactants. Li diffusivity can be dramatically enhanced when the material is mechanically treated in a high energy ball mill. LVP-0.10 exhibits the most outstanding high-rate and ultralong-life performances. The discharge capacity of 124.3 mA h g^{-1} is delivered at 20C, almost 1.5 times of that of the LVP-0 cathode (85 mA h g^{-1}). Long-life cycling performance at high rate of 20C is also exhibited, retaining 98.3% of its original discharge capacity beyond 1000 cycles. The solid state reaction technique is environmental friendly and more convenient for large-scale production, which may speed up the commercialization of LVP in high performance Li-ion batteries.

Acknowledgements

This work is supported by the National Natural Science Foundation of China (51471085, 51407029), China Postdoctoral Science Foundation (2012M520968), the International Postdoctoral Exchange Fellowship Program 2014 by the Office of China Post-doctoral Council and Scientific Research Foundation of Graduate School of Southeast University. We acknowledge fundings from Jiangsu Shuangchuang Program and the Priority Academic Program Development of Jiangsu Higher Education Institutions, and Key Laboratory of MEMS of the Ministry of Education, Southeast University.

References

1 J.-M. Tarascon and M. Armand, *Nature*, 2001, **414**, 359–367.
2 C. K. Chan, H. Peng, G. Liu, K. Mcilwrath, X. F. Zhang, R. A. Huggins and Y. Cui, *Nat. Nanotechnol.*, 2008, **3**, 31–35.
3 J. B. Goodenough and K.-S. Park, *J. Am. Chem. Soc.*, 2013, **135**, 1167–1176.
4 Y. Luo, X. Xu, Y. Zhang, Y. Pi, Y. Zhao, X. Tian, Q. An, Q. Wei and L. Mai, *Adv. Energy Mater.*, 2014, **1400107**, 1–8.
5 J. Wang and X. Sun, *Energy Environ. Sci.*, 2012, **5**, 5163–5185.
6 H. Hung, S.-C. Yin, T. Kerr, N. Taylor and L. F. Nazar, *Adv. Mater.*, 2002, **14**, 1525–1528.
7 Y. Zhou, X. Rui, W. Sun, Z. Xu, Y. Zhou, W. J. Ng, Q. Yan and E. Fong, *ACS Nano*, 2015, **9**, 4628–4635.
8 R. V. Hagen, A. Lepcha, X. Song, W. Tyrra and S. Mathur, *Nano Energy*, 2013, **2**, 304–313.
9 Q. Wei, Q. An, D. Chen, L. Mai, S. Chen, Y. Zhao, K. M. Hercule, L. Xu, A. Minhas-Khan and Q. Zhang, *Nano Lett.*, 2014, **14**, 1042–1048.
10 X. Zhang, N. Bçckenfeld, F. Berkemeier and A. Balducci, *ChemSusChem*, 2014, **7**, 1710–1718.
11 H. Liu, P. Gao, J. Fang and G. Yang, *Chem. Commun.*, 2011, **47**, 9110–9112.
12 J. Kim, J. K. Yoo, Y. S. Jung and K. Kang, *Adv. Energy Mater.*, 2013, **3**, 1004–1007.
13 C. Wang, H. Liu and W. Yang, *J. Mater. Chem.*, 2012, **22**, 5281–5285.
14 D. Han, S. Lim, Y. Kim, S. H. Kang, Y. C. Lee and Y. Kang, *Chem. Mater.*, 2014, **6**, 3644–3650.
15 M. Secchiaroli, G. Giuli, B. Fuchs, R. Marassi, M. W. Mehrens and S. Dsoke, *J. Mater. Chem. A*, 2015, **3**, 11807–11816.
16 J. S. Huang, L. Yang, K. Y. Liu and Y. F. Tang, *J. Power Sources*, 2010, **195**, 5013–5018.
17 J. Zheng, X. Li, Z. Wang, H. Guo, Q. Hu and W. Peng, *J. Power Sources*, 2009, **189**, 476–479.
18 J. Zheng, X. Li, Z. Wang, S. Niu, D. Liu, L. Wu, L. Li, J. Li and H. Guo, *J. Power Sources*, 2010, **195**, 2935–2938.
19 J. Wang, Z. Wang, X. Li, H. Guo, X. Wu, X. Zhang and W. Xiao, *Electrochim. Acta*, 2013, **87**, 224–229.
20 J. Wang, X. Li, Z. Wang, B. Huang, Z. Wang and H. Guo, *J. Power Sources*, 2014, **251**, 325–330.
21 B. Kang and G. Ceder, *Nature*, 2009, **458**, 190–193.
22 J. C. Zheng, Y. D. Han, L. B. Tang and B. Zhang, *Electrochim. Acta*, 2016, **198**, 195–202.
23 J. C. Zheng, Y. D. Han, B. Zhang, C. Shen, L. Ming and J. F. Zhang, *ACS Appl. Mater. Interfaces*, 2014, **6**, 13520–13526.
24 P. Sun, X. Wang, K. Zhu, X. Chen, X. Cui, Q. Xu, D. Su, Q. Fan and Y. Sun, *RSC Adv.*, 2017, **7**, 3101–3107.
25 P. Sun, S. Qin, X. Wang, R. An, Q. Xu, X. Cui, Y. Sun, S. Wang, P. Wang and Q. Fan, *J. Power Sources*, 2015, **293**, 922–928.
26 H. Wang, Y. Li, C. Huang, Y. Zhong and S. Liu, *J. Power Sources*, 2012, **208**, 282–287.

27 M. Wilkening, V. Epp, A. Feldhoff and P. Heitjans, *J. Phys. Chem. C*, 2008, **112**, 9291–9300.
28 M. V. Reddy, G. V. Subba Rao and B. V. R. Chowdari, *J. Mater. Chem.*, 2011, **21**, 10003–10011.
29 Y. Hao, Q. Lai, Z. Xu, X. Liu and X. Ji, *Solid State Ionics*, 2005, **176**, 1201–1206.
30 H. Chen, J. M. Wang, T. Pan, H. M. Xiao, J. Q. Zhang and C. N. Cao, *Int. J. Hydrogen Energy*, 2003, **28**, 119–124.